42nd Turbomachinery & 29th Pump SYMPOSIA

Proceedings of the Twenty-Ninth International Pump Users Symposium
October 1-3, 2013, Houston, Texas

VERTICALLY-SUSPENDED PUMPS WITH WATER-LUBRICATED RUBBER BEARINGS -- EXPERIMENTAL IDENTIFICATION OF DYNAMIC STIFFNESS COEFFICIENTS

Shibing Liu
Ph.D Student
University of Southern California
Los Angeles, California, USA

Bingen Yang
Professor
University of Southern California
Los Angeles, California, USA

Paul W. Behnke
Manager, Engineering and R&D
ITT Corporation, Goulds Pumps
City of Industry, California, USA

Lily Ding
Senior Mechanical Engineer
ITT Corporation, Goulds Pumps
City of Industry, California, USA

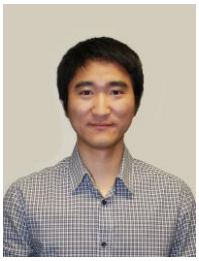

Shibing Liu is a Ph.D. student in the Department of Aerospace and Mechanical Engineering at USC. His reasearch is on modeling and dynamics of flexible rotor-bearing systems, with special interest in water-lubricated rubber bearings.

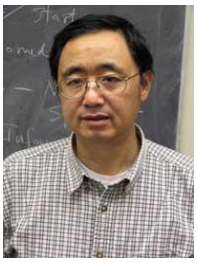

Bingen Yang is a professor of mechanical engineering at USC. With 30 years of research in structural dynamics, vibrations, and feedback controls, he has undertaken numerous projects supported by various funding agencies, including the National Science Foundation, NASA, US Army Research Office, and Ford Motor Company.

Paul Behnke (PE) is manager of engineering and R&D at ITT Corporation - Goulds Pumps. He has 33 years of experience in pump design, development, production, specification, and operation. He is a current member of the Pump Advisory Board for Turbomachinery Laboratory.

Lily (Hongli) Ding (PE, Ph.D) is a senior mechanical engineer with 20 years of research and work experience in mechanical structural analysis and fluid dynamic analysis, FEA and CFD, and mechanical design. She had worked as hydraulic engineer at ITT Goulds Pumps VPO since 2008, and currently she is working as contract consultant.

ABSTRACT

Design and development of vertically-suspended water pumps requires good understanding of the rotor system characteristics with water-lubricated rubber bearings (WLRB). This paper presents a newly-built experimental device to simulate rotor systems with WLRBs, and some initial results on experimental identification of dynamic stiffness coefficients of a long WLRB. In experiments, unbalanced mass response of a rotor system is used to determine the experimental dynamic stiffness of WLRB. The unbalanced mass response of the system is modeled by the Distributed Transfer Function Method (DTFM). Unlike traditional methods in which standard pointwise bearing models are used, the DTFM–based modeling treats a long WLRB as a viscoelastic foundation. The rubber bearing dynamic stiffness coefficients are investigated in three different cases: the rotating system carrying one disk, two disks, and three disks. The experimental results show that the WLRB dynamic stiffness coefficients increase parabolically with increasing rotating speed. In addition, the predicted natural frequencies of the rotor system by the DTFM are within eight percent of experimental results.

INTRODUCTION

Vertically-suspended pumps are used in many important applications for power generation, mining, and industrial processes. Rotor systems in these pumps are vertically oriented and have shafts which transmit both torsional and axial loads. Axial loads are produced by hydraulic forces from impellers at the bottom of the rotor system and balanced by a thrust bearing at the top of the rotor system. Between these two points of tensile load in the rotor system, radial bearings provide position control and stability to the rotating shafts at various intervals along the length of the total rotor system; see Figure 1.

Water lubricated rubber bearings (WLRBs) are often used for these radial bearings in vertically-suspended pumps pumping water. A typical WLRB is a long cylindrical metal

shell that hosts multiple rubber staves separated by axial grooves; see Figure 2. The WLRB has three major advantages: (i) pumped water used as a lubricant reduces pump cost; (ii) the water flow takes away heat and fine particles in the bearing; and (iii) the natural resilience of rubber gives the bearing good properties for shock and vibration absorption and wear resistance.

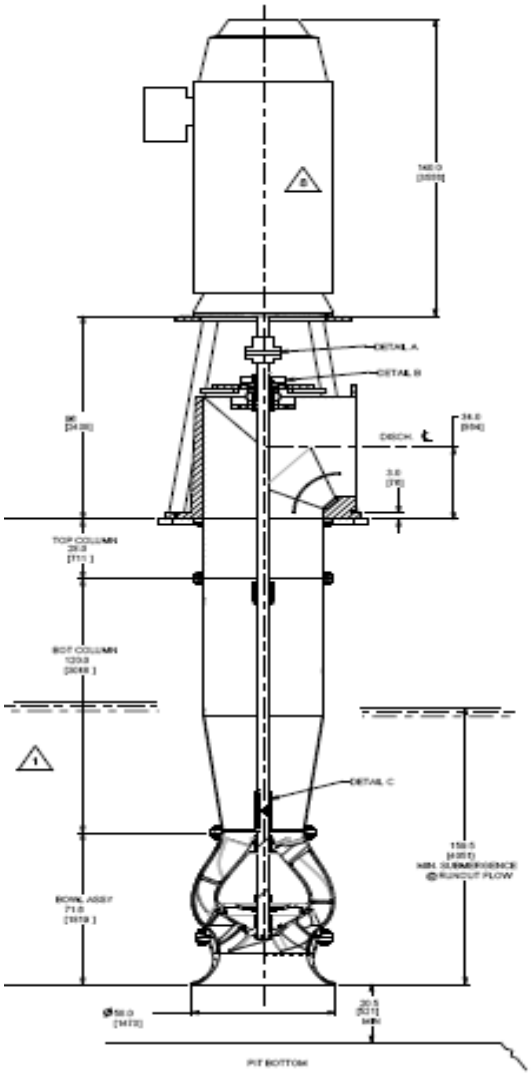

Figure 1. Typical Vertically-Suspended Pump Design with Water Lubricated Rubber Bearings

In order to improve pump reliability, pump designers calculate rotor lateral natural frequencies of the rotor systems. The results of these calculations enable designers to modify pump designs to ensure that natural frequencies are not sympathetic to the excitation frequencies applied to the rotor system, and thereby avoid "critical speeds" which cause high machinery vibration.

Many pump users understand the importance of avoiding critical speeds and therefore specify that rotor lateral natural frequency calculations shall be performed, reported, and submitted for their review and approval, as part of their pump purchase. Often pump users expect these calculations to be produced by computer-aided rotor dynamic models to enhance the accuracy of results. However, the result accuracy is mostly limited by lack dependable dynamic coefficients for WLRBs, due to a lack of faithful WLRB laboratory testing.

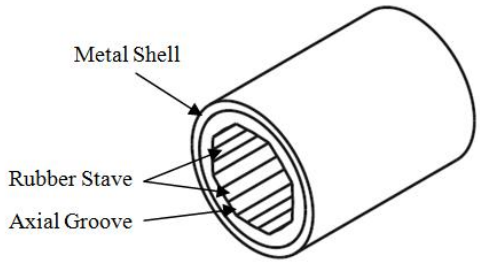

Figure 2. A Typical Water Lubricated Rubber Bearing

Existing commercial software codes on rotor dynamics are not suitable for vibration analysis of vertically-suspended pumps because they compute the dynamic coefficients of radial bearings using plain journal bearings models, and ignore the elastic deformation of rubber material, see Figure 3. Usage of current commercial rotor dynamics software codes can yield natural frequency predictions with significant differences from known historic results, and in some cases give totally wrong design direction. Using computer-aided calculations with poorly estimated dynamic coefficients for WLRBs provides pump designers and users with a false sense of confidence, and worse potentially, pump rotors operating with critical speeds and high mechanical vibration. Therefore, more accurate rubber bearing dynamic stiffness coefficients are valuable, because they could produce more reliable rotor analysis, which in turn, would produce more reliable vertically-suspended pump designs and more reliable pumping systems for pump users.

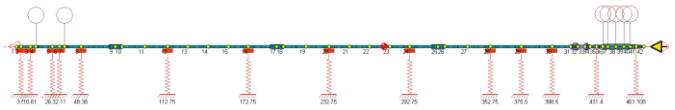

Figure 3. Vibration Analysis of a Vertical Pump with Water Lubricated Rubber Bearings

As stated by Childs (1993) and Chen (2007), long bearings can be modeled as pointwise springs and dampers by considering the pitch and yaw effects. Experimental methods for identification of dynamic coefficients of bearings have been extensively studied in the past; for instance see the review by Tiwari, et al. (2004). Dimond, et al. (2007), reviewed the methods of identification of fluid film journal bearing static and dynamic characteristics from measured data. The different force excitation methods of incremental loading, sinusoidal, pseudorandom, impulse, known/additional unbalance, and non-contact excitation were discussed. Data processing methods in the time and frequency domains were also presented. However, no experimental investigation on the dynamics stiffness coefficients of rubber bearings has been reported.

This paper presents two major results. First, a newly-built experiment device for identification of rubber dynamic stiffness and damping coefficients of WLRB is described. The device can be used to identify the rubber

bearing dynamic stiffness using a flexible rotor-rubber bearing system. To the authors' knowledge, this study is the first one that identifies the WLRB dynamic coefficients via a flexible rotor-rubber bearing system in experiments. Second, instead of commonly used pointwise bearing models, a distributed viscoelastic bearing model is introduced for long bearings like WLRB. To facilitate such a model in dynamic analysis, the Distributed Transfer Function Method (Fang and Yang, 1998) is used.

EXPERIMENTAL SETUP

The experimental identification of the dynamic stiffness coefficients of WLRB is performed by using a vertical flexible shaft-rubber bearing system. Figure 4 shows the photos of the assembly and parts of the test device. In Figure 5 is a schematic of the test device.

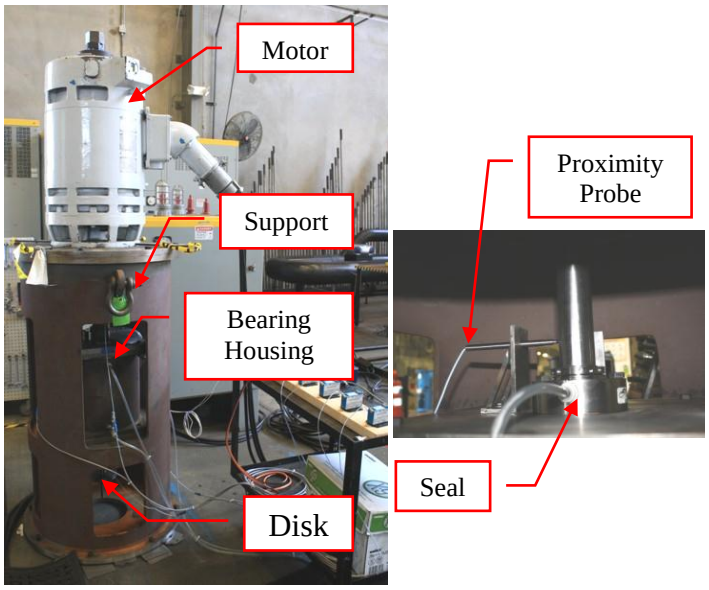

Figure 4. Water Lubricated Rubber Bearing Test Device

The test device can test one water-lubricated rubber bearing with diameters ranging from 2 to 6 inches and with a length-to-diameter ratio of 2. The liner material of rubber bearings is Nitrile. Corresponding rotating journal sleeves are made of polished stainless steel and mounted on a shaft, which is adjustable to be concentric with the rubber bearing centerline. At the lower end of the shaft is a disk with four symmetric holes, which is used to introduce unbalanced mass to the rotor. To lubricate the bearing, city water flows through the running clearance by injection to the water inlet and collection from the water outlet; see Figure 5. Because the water inlet is lower than the water outlet, the bearing house is always completely filled with water, making water fully functioning as a lubricant during the operation of the test device.

The bearing housing is sealed by two face-type mechanical seals, whose radial forces applied on the shaft is neglectable. Four proximity probes that are mounted above and below the bearing housing are used to measure the vibration displacements of the rotating shaft in x- and y- directions. A data acquisition system (Figure 5) records pressure and vibration measurements. Based on these measurements, the natural frequencies of the flexible rotor-bearing system are determined.

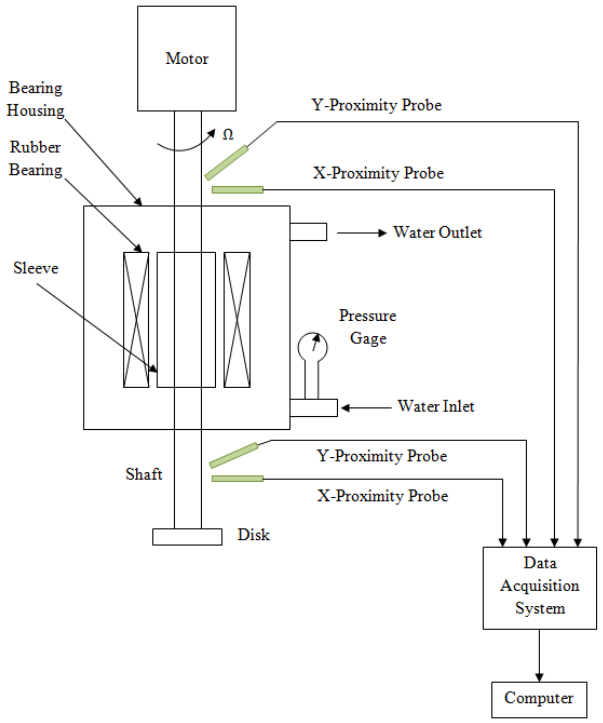

Figure 5. Schematic of the Water Lubricated Rubber Bearing Test Device

APPROACH

Unbalanced mass response is used to determine the dynamic stiffness of WLRBs. Experimental unbalanced response, in both time and frequency domain, of the rotor - 4 inches rubber bearing was recorded using four proximity probes. The theoretical unbalanced mass response is derived using DTFM. The unknown rubber bearing dynamic stiffness coefficients are solved by matching the experimental and theoretical unbalanced mass response.

Unbalanced mass is mounted to one of the holes of the disk. Theoretically, unbalanced mass response of a rotor system only consists of the frequency that equals to 1X running speed. However, from the experimental results, the recorded frequency response always shows higher harmonic frequencies. The higher harmonic frequencies can be result of the misalignment. But, the amplitude of the higher harmonic response is very small, compared with that of the frequency that equals to 1X running speed. To get the pure 1X running speed frequency from the recorded response, complex variable filtering method was used. Complex variable filtering method was explained by Consulting (2005). The goal of complex variable filtering is to separate the frequency components contained in a rotor orbit into circular, forward and reverse frequency components. Following the procedure of complex variable filtering method, the experimental 1X-filtered orbit can be written as

$$\begin{pmatrix} u \\ v \end{pmatrix} = \begin{bmatrix} a_1 & b_1 \\ a_2 & b_2 \end{bmatrix} \begin{pmatrix} \cos\Omega t \\ \sin\Omega t \end{pmatrix} \quad (1)$$

where u and v are the experimental vibration amplitudes in x and y direction; a_1, b_1, a_2 and b_2 are coefficients obtained from the complex variable filtering method; Ω is the rotating speed.

The Distributed Transfer Function Method (DTFM) is a powerful method for modeling, analysis and control of flexible dynamic systems. One obvious advantage of the DTFM over traditional finite element methods (FEM) is that it can deliver highly accurate solutions of dynamic problems without the need for discretization. As another advantage, the DTFM is convenient for computer coding, and efficient in numerical simulation. The DTFM for one-dimensional distributed parameter systems was first time studied by Yang and Tan (1992). Later, Fang and Yang (1998) applied the DTFM to complex flexible rotor systems. The DTFM used in this paper is further developed from Fang and Yang's (1998) method.

To model long rubber bearings, the deformation of the rubber surface should be considered. However, pointwise bearing model cannot precisely represent the characteristics of long rubber bearings. In this paper, a shaft segment with long WLRB is modeled as the rotating beam segment supported by viscoelastic foundation, which is called distributed bearing model. Distributed bearing model assumes the long bearing is divided into infinity short bearings. Each short bearing is modeled as spring and damper. Then, the long bearing can be approximated as visoelastic foundation including the stiffness and damping effects (Figure 6).

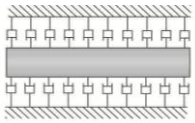

Figure 6. Distributed Model of Long WLRB

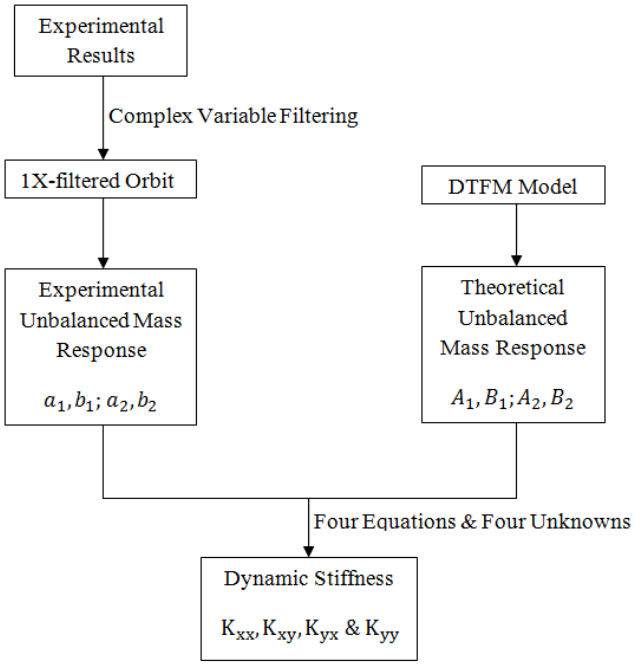

Figure 7. Data Processing Procedure

By the DTFM as described in the Appendix, the unbalanced mass response of a flexible rotor-bearing system can be written as

$$\begin{pmatrix} U \\ V \end{pmatrix} = \begin{bmatrix} A_1 & B_1 \\ A_2 & B_2 \end{bmatrix} \begin{pmatrix} cos\Omega t \\ sin\Omega t \end{pmatrix} \quad (1)$$

where U and V is the theoretical vibration amplitude in x and y direction; A_1, B_1, A_2 and B_2 are coefficients obtained from the DTFM. Comparing Equation (1) and Equation (2) yields

$$\begin{bmatrix} a_1 & b_1 \\ a_2 & b_2 \end{bmatrix} = \begin{bmatrix} A_1 & B_1 \\ A_2 & B_2 \end{bmatrix} \quad (2)$$

There are four equations and four unknowns, which are the four dynamic stiffness coefficients of the rubber bearing (i.e. K_{xx}, K_{xy}, K_{yx} & K_{yy}), in Equation (3). Then, the rubber bearing dynamic stiffness coefficients can be determined. A flow chart of the data processing procedure is shown in Figure 7.

Boundary Conditions

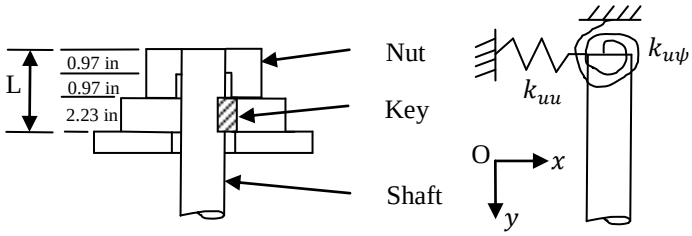

Figure 8. Top Boundary of the Rotor-Bearing System

In analyzing test results, it is found that the boundary condition within the system model representing a keyed connection between the motor and shaft at the top of the test device is an important factor affecting the results. This next section introduces how to model the boundary conditions, especially the top boundary condition.

The bottom boundary condition of the model is simple, because the bottom end of rotor in the test device is free. The top boundary condition of the model however is complex, because the shaft is fastened by a nut and driven by a key, as shown in Figure 8.

The top boundary cannot be modeled as simply supported or clamped, because neither represents the top boundary condition precisely. In this paper, the top boundary is modeled as springs which generate constraints in both translational and torsional direction. As pointed out by Friswell, et al. (2010), the spring force can be determined as

$$f_x = k_{uu}U + k_{u\psi}\frac{\partial U}{\partial z};\ f_y = k_{vv}V - k_{v\theta}\frac{\partial V}{\partial z} \quad (3)$$

where $k_{uu}, k_{u\psi}, k_{vv}$ and $k_{v\theta}$ are stiffness coefficients of the equivalent spring; k_{uu} is the force in the direction Ox required to produce a unit displacement u when no other displacements or rotations are allowed to occur; $k_{u\psi}$ is the force in the direction Ox required to produce a unit rotation ψ when no other displacements or rotations are allowed to occur. The spring stiffness is assumed to be equal to the equivalent spring stiffness of the upper shaft with length L. The equivalent spring stiffness of the upper shaft can be derived from Finite Element Method (FEM), which are

$$k_{uu} = k_{vv} = \frac{12EI}{l^3};\ k_{u\psi} = -k_{v\theta} = -\frac{6EI}{l^2} \qquad (4)$$

where E and I is the Young's modulus and moment of inertial of the shaft, respectively; l is the effective length of the shaft at the top boundary, which is 3.20 inches.

The obtained boundary conditions will be implemented in the Distributed Transfer Function Method based rotor-bearing model.

RESULTS

In the following results, a rubber bearing with inside diameter of 4.010 inches, length of 8.00 inches, and a corresponding journal sleeve with outside diameter of 3.998 inches are used, resulting in nominal diametrical clearance of 0.012 inches. The unbalanced mass response of the flexible rotor-bearing system is recorded for three different cases: the shaft carrying one disk, two disks, and three disks. The supply pressure is kept as constant. The rotating speed varies from 600 rpm to 1700 rpm. Due to the limitation of the data acquisition system, the maximum vibration amplitude that the data acquisition system can record is 0.015 inches. And, the experimental data can only be taken up to 1350 rpm for the two-disks case and 1150 rpm for the three-disks case.

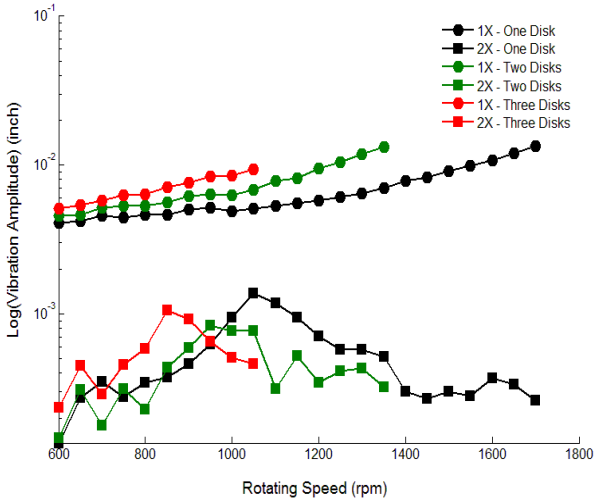

Figure 9. Unbalanced Mass Response

Experimental Unbalanced Mass Response

The unbalanced masses weigh 0.08 lb, 0.095 lb, and 0.1 lb for the cases of one disk, two disks, and three disks, respectively. The unbalanced mass response of the three cases is shown in Figure 9. The 1X running-speed and 2X running-speed components of vibration are recorded separately using complex variable filtering. As expected, the 1X running-speed response increases as the rotating speed increases. But unexpectedly, responses at 2X running-speed are also recorded. The peak displacement occurs at 1050rpm, 950rpm and 850 rpm for the case with one disk, two disks, and three disks, respectively. During testing, resonance is observed at these rotating speeds. However, the highest vibratory amplitudes appear at 2X running-speed, not at 1X. This indicates that the natural frequency of the rotor system equals the 2X running speed. In another words, the natural frequencies of the rotor system with one disk, two disks, and three disks are 35.00Hz, 31.67Hz and 28.33Hz, respectively. Because the 1X running-speed response is much higher than the 2X running-speed response, the unbalance mass response of the system is approximately equal to the 1X running-speed response. It follows that the unbalanced mass response of the system is approximately proportional to the imbalance amplitude.

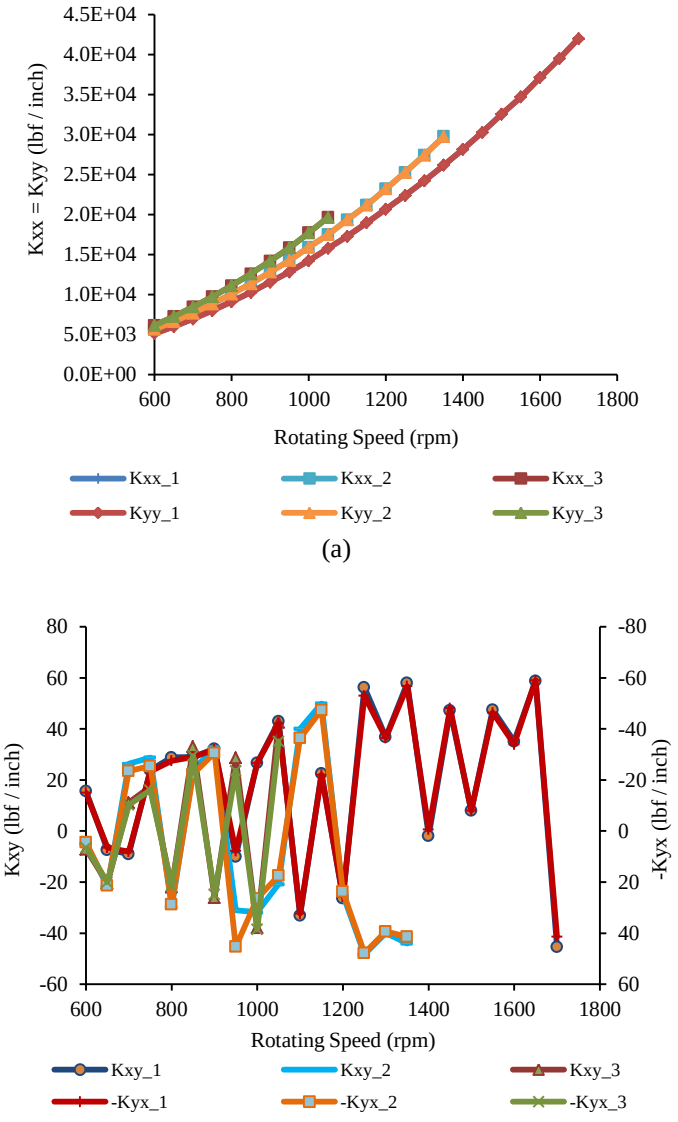

Figure 10. Dynamic Stiffness of the Rubber Bearing (a) Direct Stiffness; (b) Cross Coupled Stiffness (Note: Number 1, 2 and 3 represents the case with one disk, two disks and three disks, respectively)

Dynamic Stiffness Coefficients

The rubber bearing dynamic stiffness coefficients are determined using Equations (1) - (3). As can be seen from Figure 10, $K_{xx} = K_{yy}$ and, at most points, $K_{xy} \approx -K_{yx}$. Generally, the direct stiffness coefficients increase as a parabola type with respect to the rotating speed. From Figure 10a, it can be seen that the direct stiffness for the three cases is similar with each other. But, in Figure 10b, the cross coupled stiffness is different for the three cases even though some points overlap. There is no significant relationship between the cross coupled stiffness and the rotating speed.

As stated by Vance, et al. (2012), the cross coupled dynamic stiffness coefficients that produce forces tangential to the whirl orbit have little effect on natural frequencies. They mainly affect stability and amplification factors at a critical speed. Even though the determined cross coupled stiffness coefficients for the three cases are different, the natural frequency of the system can still be predicted without the cross coupled stiffness coefficients.

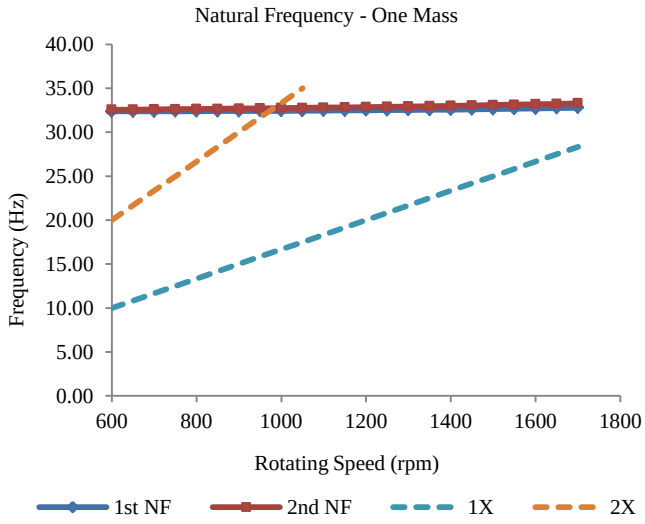

(a)

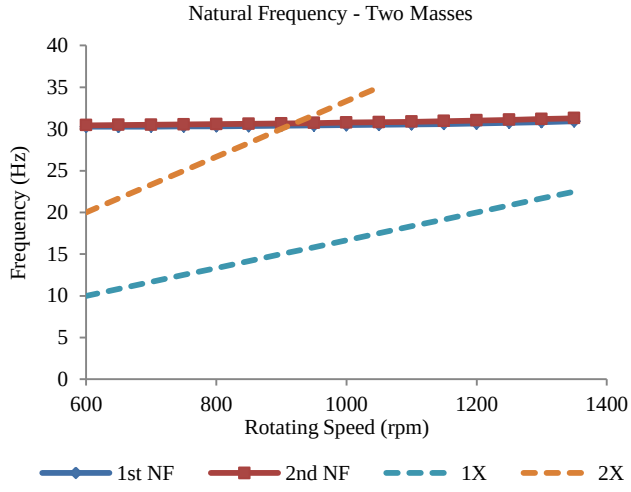

(b)

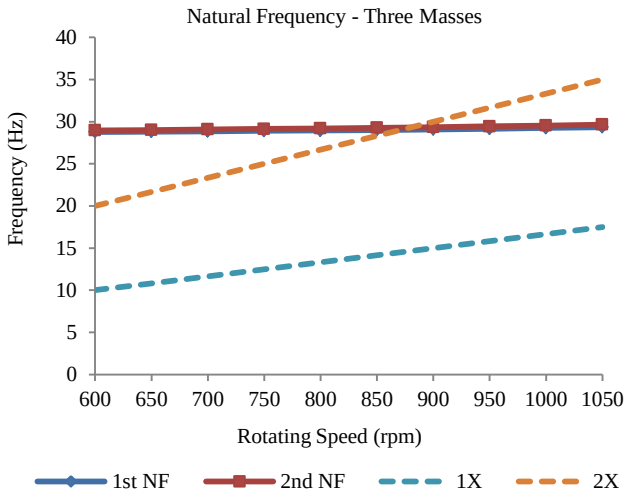

(c)

Figure 11. Campbell Diagram of the Rotor-Bearing System (a) One Disk; (b) Two Disks; (c) Three Disks

Table 1 Theoretical and Experimental Natural Frequency

Cases	Theoretical Natural Frequency (Hz)		Experimental Natural Frequency (Hz)	Error	
	1st	2nd		1st	2nd
One disk at 1050 rpm	32.44	32.77	35.00	7.3%	6.3%
Two disks at 950 rpm	30.42	30.70	31.67	4.0%	3.1%
Three disks at 850 rpm	29.02	29.27	28.33	2.4%	3.3%

Natural Frequencies

The theoretical natural frequencies of the system can be predicted by using the determined dynamic stiffness coefficients with DTFM. The Campbell diagram for the three cases is shown in Figure 11.

It is obvious that the 2X running-speed line crosses the first and second natural frequency. This indicates that the periodic force with 2X running-speed frequency can excite resonance at this point. As stated previously, this resonance is observed during the experiment. From the experiment results, resonance occur at 1050 rpm for the case with one disk; 950 rpm and 850 rpm for the cases with two disks and three disks, respectively. However, the experimental resonance is observed on the 2X running-speed frequency response. This

is consistent with the theoretical prediction. The theoretical and experimental natural frequencies for the three cases are summarized in Table 1. Since the first and second natural frequencies are very close to each other, it is unknown that which natural frequency is excited. So, the experimental natural frequencies are compared with both the first and second natural frequencies. It is concluded that the theoretical natural frequencies match the experimental frequency very well.

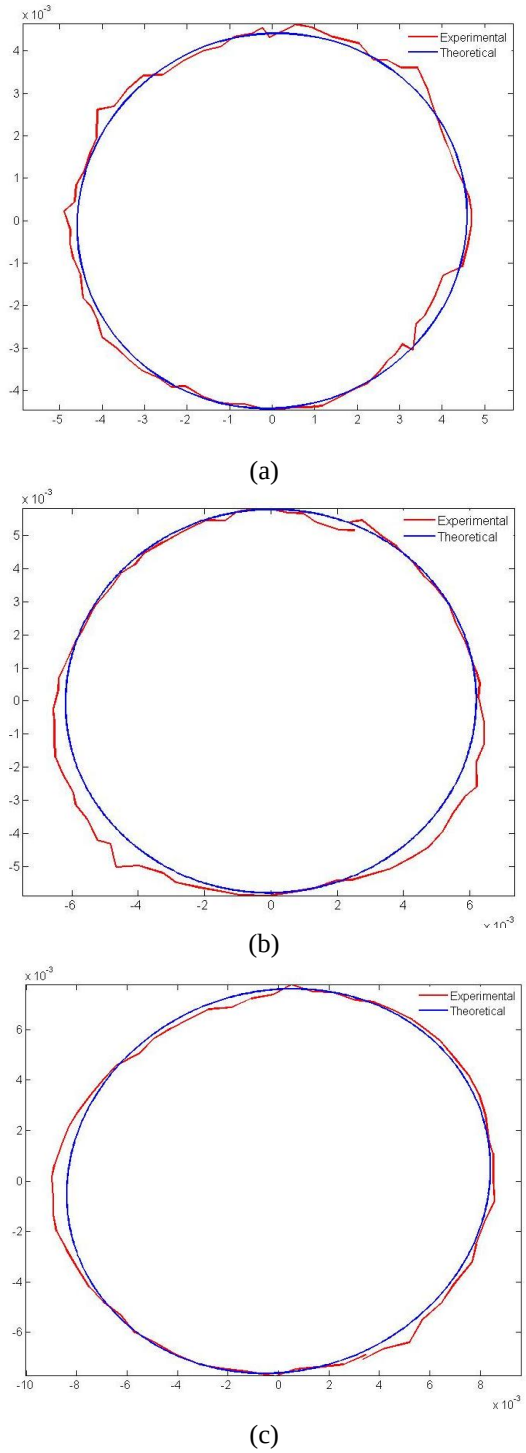

Figure 12. Comparison of Theoretical and Experimental Unbalanced Mass Response at the lower proximity probe at (a) 800rpm for the case with one disk; (b) 900rpm for the case with two disks; (c) 1000rpm for the case with three disks

Theoretical Unbalanced-Mass Response

The theoretical unbalanced-mass response (2-D trajectory) is calculated through use of the determined rubber bearing dynamic stiffness coefficients and the DTFM. The experimental and theoretical unbalanced mass response at the lower proximity is compared in Figure 12. At most points, the theoretical and experimental unbalanced mass response match with each other very well.

CONCLUSIONS

The newly-built experimental device is shown to be useful for investigation of the behaviors of long WLRBs. The initial results obtained on this test device identify dynamic stiffness coefficients of WLRBs, and will enable future testing of these types of bearings.

From the experimental data, the direct bearing stiffness (K_{xx}, K_{yy}) for the three cases show similar trends. But, the cross coupled stiffness (K_{xy}, K_{yx}) and the rotating speed does not show significant relationship. Since the theoretical and experimental natural frequency and unbalanced mass response match with each other very well, it can be concluded that the determined dynamic stiffness coefficients of water lubricated rubber bearings are very precise. In this paper, only test results for the 4-inch rubber bearing are presented. In future, 2-inch and 6-inch rubber bearings should be studied to develop a general theoretical rubber bearing model. And damping coefficients of long water lubricated rubber bearings will be determined in the follow-up investigations, in order to fully understand the dynamics of flexible shaft-bearing systems.

NOMENCLATURE

u	= Experiment vibration amplitude in x-axis
v	= Experiment vibration amplitude in y-axis
a_1, b_1, a_2, b_2	= Coefficients obtained from the complex variable filtering method
U	= Theoretical vibration amplitude in x-axis
V	= Theoretical vibration amplitude in y-axis
A_1, B_1, A_2, B_2	= Coefficients obtained from the DTFM
$K_{xx}, K_{xy}, K_{yx}, K_{yy}$	= Rubber spring stiffness coefficients
$C_{xx}, C_{xy}, C_{yx}, C_{yy}$	= Rubber bearing damping coefficients
q_x, q_y	= Bearing forces
f_x, f_y	= Equivalent of the spring force of the top boundary
$k_{uu}, k_{u\psi}, k_{vv}, k_{v\theta}$	= Equivalent spring stiffness coefficients of the top boundary
l	= Effective length of the shaft at the top boundary
E	= Young's modulus of the shaft
I	= Moment of inertial of the shaft
ρ	= Shaft density
A	= Shaft cross-section area
L_e	= Length of shaft segment
F_x, F_y	= External force applied of shaft
$G(z, \xi, s), H(z, s)$	= Distributed transfer functions
$\gamma(s)$	= Modal displacements at the two ends of the shaft segment

REFERENCES

Muszynska, Agnes, 2005, "Rotordynamics," CRC Press, Taylor & Francis Group.

Chen, W. J. and Gunter, E. J., 2007, "Introduction to Dynamics of Rotor-Bearing System," Trafford Publishing.

Childs, D. W., 1993, "Turbomachinery Rotordynamics: Phenomena, Modeling, and Analysis," Wiley-Interscience.

Dimond, T. W., Sheth, P. N., Allaire, P. E. and He, M., 2009, "Identification Methods and Test Results for Tilting Pad and Fixed Geometry Journal Bearing Dynamic Coefficients - A Review," Shock and Vibration, 16, 13-43.

Fang, H. and Yang, B., 1998, "Modeling, Synthesis and Dynamic Analysis of Complex Flexible Rotor System," Journal of Sound and Vibration, 211, 571-592.

Friswell, M. I., Penny, J. E. T., Garvey, S. D. and Lees, A. W., 2010, "Dynamic of Rotating Machine," Cambridge University Press.

Tiwari, R., Lees, A. W. and Friswell, M. I., 2004, "Identification of Dynamic Bearing Parameters: A Review," The Shock and Vibration Digest, 36, 56-67.

Vance, J., Zeidan, F. and Murphy, B., 2012, "Machinery Vibration and Rotordynamics," John Wiley & Sons, Inc.

Yang, B. and Tan, C.A., 1992, "Transfer Functions of One-Dimensional Distributed Parameter Systems," ASME Journal of Applied Mechanics, 59, 1009-1014.

APPENDIX: The Distributed Transfer Function Method for Moldeling and Anlaysis of Flexible Rotor-Bearing Systems

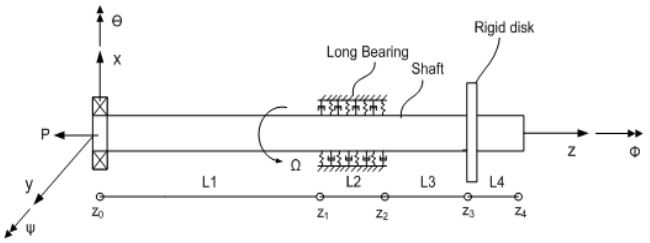

Figure A1. Schematic of the flexible rotating shaft with a long bearing and mounted disk

In Figure A1 is the schematic of a flexible rotating shaft-bearing system. In the DTFM, divide the shaft into a number of segments by nodes $z_0, z_1, z_2 \ldots$, which are the locations of mounted rigid disks, boundaries of long bearings, and the ends of the shaft. Unlike in FEM modeling, the segment length L_i does not have to be small. The rotor-bearing system thus has three basic elements as shown in Fig. A2: shaft segment with or without long bearings, and mounted rigid disks.

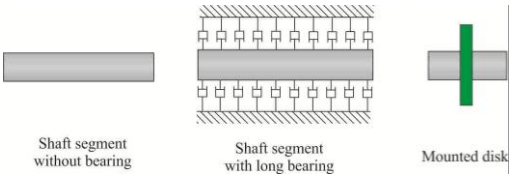

Figure A2. Basic elements of the rotor-bearing system

As a demonstrative example consider the Rayleigh beam theory for a rotating shaft segment. The governing equations of motion of the shaft segment are

$$EI\frac{\partial^4 u}{\partial z^4} - 2\rho I\Omega\frac{\partial^3 v}{\partial z^2\partial t} - \rho I\frac{\partial^4 u}{\partial z^2\partial t^2} + \rho A\frac{\partial^2 u_i}{\partial t^2} = F_x + q_x$$
$$EI\frac{\partial^4 v}{\partial z^4} + 2\rho I\Omega\frac{\partial^3 u}{\partial z^2\partial t} - \rho I\frac{\partial^4 v}{\partial z^2\partial t^2} + \rho A\frac{\partial^2 v}{\partial t^2} = F_y + q_y \qquad \text{(A1)}$$

where Ω is the rotation speed of the shaft, $u(z,t)$ and $v(z,t)$ are the transverse displacements of the shaft, F_x *and* F_y are the external force applied on the shaft, and q_x and q_y are the bearing forces of the form

$$q_x = -C_{xx}\frac{\partial u}{\partial t} - C_{xy}\frac{\partial v}{\partial t} - K_{xx}u - K_{xy}v$$
$$q_y = -C_{yx}\frac{\partial u}{\partial t} - C_{yy}\frac{\partial v}{\partial t} - K_{yx}u - K_{yy}v \qquad \text{(A2)}$$

with $C_{\alpha\beta}$ and $K_{\alpha\beta}$ being the dynamic coefficients of the bearing, which in general are functions of z. Unlike conventional pointwise bearing models, Eqs. (A1) and (A2) are v for bearings with a large length-to-diameter ratio.

By taking Laplace transform of Equation (6), Eqs. (A1) and (A2) can be casted into the spatial state form

$$\frac{\partial}{\partial z}\{\hat{\eta}(z,s)\} = [F(z,s)]\{\hat{\eta}(z,s)\} + \{p(z,s)\} \qquad \text{(A3)}$$

where

$\{\hat{\eta}(z,s)\} = \{\bar{u}, \bar{u}', \bar{u}'', \bar{u}''', \bar{v}, \bar{v}', \bar{v}'', \bar{v}'''\}^T$

$\{p(z,s)\} = \{0,0,0, q_x(z,s)/EI, 0,0,0, q_y(z,s)/EI\}^T$

$[F(s)]$ is an eight-by-eight state matrix

the over-bar stands for Laplace transformation with respect to t, s is the complex Laplace transform parameter, and $\bar{u}' = \partial\bar{u}/\partial z$. By the DTFM (Yang and Tan, 1992; Fang and Yang,1998), the s-domain solution of Equation (A3) can be expressed by

$$\{\hat{\eta}(z,s)\} = \int_0^{L_e}[G(z,\xi,s)]\{p(\xi,s)\}d\xi + [H(z,s)]\{\gamma(s)\} \qquad \text{(A4)}$$

where L_e is the length of the shaft segment, $G(z,\xi,s)$ and $H(z,s)$ are the distributed transfer functions that can be obtained in exact and closed form, and $\gamma(s)$ contains the modal displacements at the two ends of the shaft segment.

Finally, by Eq. (A4), the unbalanced mass response of a flexible rotor-bearing system can be written as

$$\begin{pmatrix} U \\ V \end{pmatrix} = \begin{bmatrix} A_1 & B_1 \\ A_2 & B_2 \end{bmatrix}\begin{pmatrix} cos\Omega t \\ sin\Omega t \end{pmatrix} \qquad \text{(A5)}$$